VOL. 17, NO. 8, APRIL 2022 ISSN 1819-6608
ARPN Journal of Engineering and Applied Sciences

www.arpnjournals.com

SYNTHESIS BY A TWO-STEP METHOD OF THE THIN FILM SEMICONDUCTOR $CsPbBr_3$

T. Muñoz[1], G. Gordillo[2], M. A Reinoso[3], J. I Clavijo Penagos[1] and O. G. Torres[2]
[1]Departamento de Química, Universidad Nacional de Colombia, Bogotá, Colombia
[2]Departamento de Física, Universidad Nacional de Colombia, Bogotá, Colombia
[3]Facultad de Ciencias de la Ingeniería, Universidad Estatal de Milagro, Guayaquil, Ecuador
E-Mail: ogtorresd@unal.edu.co

ABSTRACT

Thin films of $PbBr_2$ were synthesized on glass substrate by Physical Vapor Deposition (PVD) and thin films of $CsPbBr_3$ were synthesized by Dip Coating Method of a film of $PbBr_2$ in a solution of CsBr in methanol. The crystalline system corresponding to $CsPbBr_3$ was identified crystallographically by X-ray diffraction and the desired stoichiometry was found from a three-dip test with a film anneal time at 100 ° C for a time of 20 minutes. The morphology of the $PbBr_2$ and $CsPbBr_3$ films was studied by scanning electron microscopy (SEM), the structural change and the variation in grain size were analyzed as a function of the annealing temperature and the formation of $CsPbBr_3$, an increase was observed in the grain size after the annealing of the $PbBr_2$ film and subsequently in the formation of $CsPbBr_3$. Finally, the optical properties of the material were evaluated by optical reflectance measurements and an optical band gap of 2.31 eV and absorption coefficients of $6x10^4$ cm^{-1} were obtained for the fundamental absorption and $5x10^4$ cm^{-1} for the near ultraviolet. The band gap of the material was also determined using the band structure diagram obtained from Heyd-Scuseria-Ernzerhof (HSE) density functionalities and a value of $2.30\ eV$ was obtained.

Keywords: semiconductor, lead halide perovskite, thin films, Kubelka-Munk transform, Tauc plot, optical properties.

INTRODUCTION

There are several materials that have been studied to take advantage of electromagnetic radiation of sun. These studies seek to improve the parameters and conditions necessary for said material to absorb this type of energy and this energy can be used later in solar cell [1]. Monocrystalline silicon is a widely used material for the manufacture of solar cells due to its great abundance, it has a band gap of 1.12 eV and a conversion efficiency of around 24% [2]. Despite the qualities of silicon cells, various materials have been studied and synthesized in thin film that have suitable properties as an absorbent layer for solar cells. The synthesis in thin film lies in the reduction of costs in the photovoltaic generation of electrical energy through the use of manufacturing processes of solar modules and cheap materials compared to silicon [3].

The materials that have been studied as an absorbent layer have constituted various types of solar cells, including perovskite-type cells. This material had a significant increase in the number of investigations since 2014 because it has presented promising results for the manufacture of solar cells. Commonly used perovskites are so-called 3D perovskites with a common ABX_3 crystal structure, where A is a monovalent cation (organic or Cs^+), B is a divalent metal that is typically Pb, and X is a halogen, typically I, Br, or Cl [4]. The record efficiency of Perovskite solar cells (PSC) has been improved from 9.7% to 20.1% [5]. These results have been achieved due to the investigation of absorbent layers such as the salts of $CH_3NH_3PbI_3$ and $CsPbX_3$. However, the use of cesium instead of the methylammonium group $CH_3NH_3^+$ allows to obtain more stable structures with respect to temperature and humidity [6]. $CsPbX_3$ perovskites have been important for applications in solar cells because they exhibit a direct band gap and large absorption coefficients (up to $2.4\times10^5 cm^{-1}$) in the UV range [7], their importance is due to the fact that these properties are key in the performance of an absorbent layer in a solar cell. The development of solar cells with an active layer of a thin film of perovskite became one of the most promising technologies for the application of solar energy in recent years [6].

Traditional techniques for the synthesis of these materials, such as vacuum evaporation and sputtering, are adequate but highly expensive and resource-consuming techniques; while the precursor solution film growth techniques are low-cost and easy-to-implement chemical synthesis techniques. The Dip Coating technique is the most widely used for industrial and especially laboratory applications, which is essentially based on simple processing, low cost and high quality of the coating [8].

EXPERIMENTAL

Thin Film Synthesis

The cleaning of the glass substrates was carried out in a sulfochromic mixture, a polarity bath (acetone, ethanol and deionized water), immersion of the glasses in alconox at 60 ºC and an ultrasound cleaning in each of the washing steps for 10 minutes. Finally, the glasses were dried with N_2 (gas). For thin film synthesis, a $PbBr_2$ thin film (0.3 g) is initially manufactured on a glass substrate by thermal evaporation under vacuum ($1.8x10^{-5}$ mbar). Once the thin films of $PbBr_2$ have been obtained, the Dip Coating technique is used, which consists of immersing a glass substrate covered with $PbBr_2$ at room temperature in a precursor solution of CsBr in methanol (5 mg/mL). The first three immersion tests were carried out for a time of 10

minutes and the fourth test consisted of a time of 20 minutes for each immersion. After each immersion, the film is annealed at 100ºC for 20 minutes. The Dip Coating technique was performed with a low-cost prototype.

Characterization

X-ray diffraction measurements are performed on a Shimadzu RX 6000 equipment for the different $CsPbBr_3$ thin film synthesis assays. The surface morphology of the $PbBr_2$ films and the material of interest was studied using a TESCAN VEGA Scanning Electron Microscope (SEM) and the results were analyzed taking into account thermal annealing and CsPbBr3 synthesis. The optical properties of the $CsPbBr_3$ thin films were evaluated by optical reflectance measurements at room temperature and using a wavelength scan from 300 to 2000 nm in a UV-Vis-NIR Shimadzu UV-3600 equipment. Finally, the thickness of the thin films was measured using a Veeco Dektak 150 profilometer.

RESULTS AND DISCUSSIONS

X-Ray Diffraction

The crystallographic identification of the material was carried out by XRD and the experimental diffraction pattern (Figure-1-D) was compared with a reference pattern obtained by means of the Crystal Impact Match Software database. Diffraction peaks corresponding to $CsPbBr_3$ are found for an orthorhombic crystal system. The most representative diffraction signals obtained are found at 2θ: 15.2º, 21.4º, 30.6º, 34º, 37.8º, 43.7º, associated with the planes (101), (121) and (202) for the first three peaks respectively. These peaks noted above are clearly present in the desired material with a 1:1 stoichiometric ratio, confirming the presence of the dominant perovskite phase $CsPbBr_3$ [9].

The immersion tests carried out for the synthesis of the material show that the immersion time is an important variable to obtain the stoichiometry of $CsPbBr_3$. By X-ray diffraction, the influence of the immersion time on the formation of the thin film can be observed. Figure 1-d shows that the formation of $CsPbBr_3$ is obtained for a test of three immersions of the substrate in the CsBr solution, each with an immersion time of 20 minutes. In Figure 1-c the characteristic peaks of the material begin to be representative and suggest that the formation of the material of interest is taking place. For Figures 1-a and 1-b we find diffraction peaks at 11.7º, 23.48º and 11.6º, 23.34º respectively that correspond to other crystalline phases. The diffraction peaks located around 12.88º and 23.15º indicate the presence of crystalline phases of $CsPb_2Br_5$ [10], which has a tetragonal crystal system. The presence of $CsPb_2Br_5$ is attributed to the perovskite-based crystallization process that occurs during the preparation of the thin film on the substrate [11]. For the analysis of the synthesis of $CsPbBr_3$ we have that $PbBr_2$ is an insoluble compound in methanol, so the immersion does not affect its film. The formation of $CsPbBr_3$ occurs through the interaction of Cs^+ and Br^- ions in solution with the surface of a film of $PbBr_2$ and $CsPb_2Br_5$ between the p orbitals of lead and bromine and s of cesium. Initially there is an absorption of these ions in the material, their formation after absorption can be given by nucleation processes. Increasing the concentration of ions in the film leads to a phase change of a material with a tetragonal crystal system (due to $PbBr_2$) that is observed in the peaks of diffractograms Figure-1-a and 1-b, to a crystalline system orthorhombic corresponding to $CsPbBr_3$. Temperature and Pb_2^+ concentration are two key factors for the formation of $CsPbBr_3$/$CsPb_2Br_5$ mixtures [11]. Thermal annealing is necessary in most deposition techniques to remove residual solvents or additives and adjust the desired stoichiometry, it has been shown that an annealing temperature between 80ºC and 100ºC is optimal for the morphology of the film and the time of annealing influences the formation of pure crystalline phases.

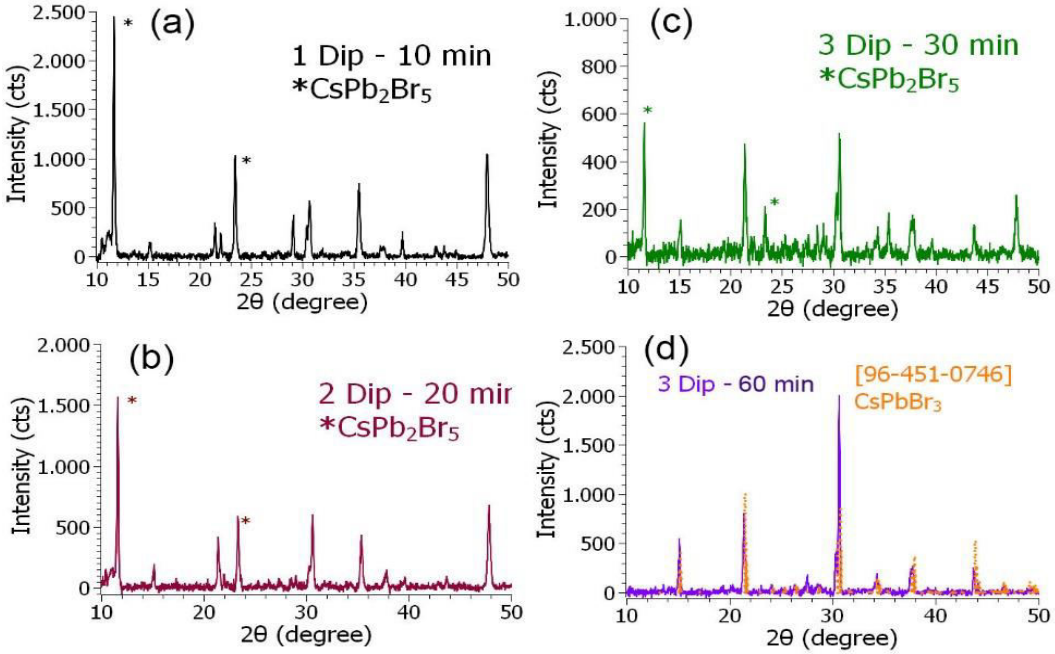

Figure-1. XRD of thin films synthesized by Dip Coating. (a) One immersion of thin film PbBr2 in BrCs solution for 10 minutes (b) Two immersion of thin film PbBr2 in BrCs solution for 10 minutes each (c) Three immersion of thin film PbBr2 in BrCs solution for 10 minutes each (d). Three dives of thin PbBr2 in BrCs solution for 20 minutes each.

Morphological Properties

Figures-2-a,b show the image obtained by scanning electron microscopy of the $PbBr_2$ film synthesized by thermal evaporation before and after annealing, respectively. An adequate $PbBr_2$ coating on the substrate is observed by this thin film synthesis method and an increase in grain size in intervals mostly between 0.08-0.12 µm to a range of 0, 10-0.30 µm according to the histogram. A larger grain size distribution is observed in the Figure-2-b histogram compared to the $PbBr_2$ film prior to thermal annealing; this observed Grain size distribution only suggests random growth or possibly random orientation in grain growth. Finally, $PbBr_2$ films with a thickness of 300 nm are obtained.

The morphology of thin film CsPbBr3 is observed in Figure-2-c in which there is a significant increase in the grain size with lengths to a greater extent from 0.5 µm to 2.0 µm and there is no formation of small grains. The significant change in grain size and its distribution may indicate the synthesis of a material other than the PbBr2, Finally a film thickness of 600 nm is obtained.

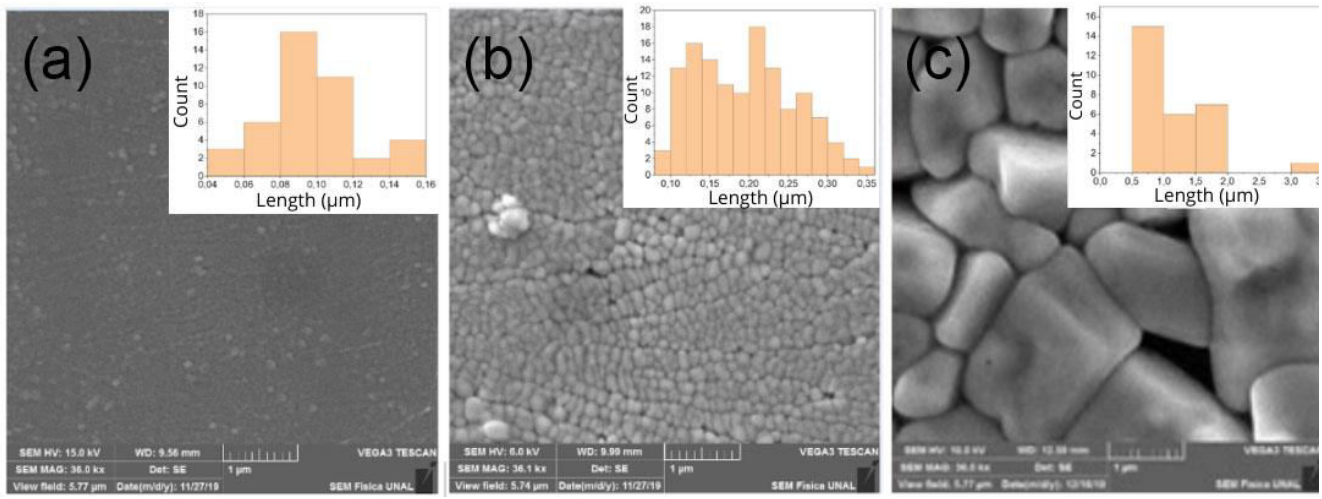

Figure-2. Scanning electron microscopy (SEM) of (a) $PbBr_2$ thin film synthesized by thermal evaporation, (b) $PbBr_2$ film after annealing at 200ºC, (c) $CsPbBr_3$ thin film after annealing at 100ºC.

Computational Calculations

A cubic crystal structure of CsPbBr3 with lattice parameters of 6.017 Å is constructed, which is structurally refined and minimized with the Quantum Espresso Suite of programs. An orthorhombic crystalline system and band structures are obtained (using Heyd-Scuseria-Ernzerhof (HSE) density functionalities, this functional allows to correctly represent the electronic structure of the material). These results are observed in Figures 3 and 4 respectively. A direct forbidden band is observed in the $CsPbBr_3$ band structure, since the maximum of the valence band and the minimum of the conduction band coincide at the point Γ of high symmetry in the Brillouin zone, where the probability of the transition electronics is higher. When the maximum of the valence band occurs in the same wave vector as the minimum of the conduction band, we have a direct semiconductor [12]. In Figure-3 we observe the band structure found at the symmetry points of a primitive cell and from which it is possible to determine the band gap of the material. The band gap calculated by this process has a value of 2.3 eV, which was corroborated with the optical band gap obtained experimentally. The relatively large bandgap of $CsPbBr_3$ films can limit their use as an active layer in a photovoltaic device. However, it is a material to which other halogens such as iodine can be substituted to obtain perovskites of the $CsPbBr_{3-x}I_x$ type with ($0 \leq x \leq 1$) to which a smaller band gap can be adjusted [13]. Materials that have a higher energy absorption of photons such as $CsPbBr_3$ perovskite can also be used in tandem cells [14] in which there are more junctions of other materials that absorb the photons that are transmitted and thus a complementary absorption can be obtained.

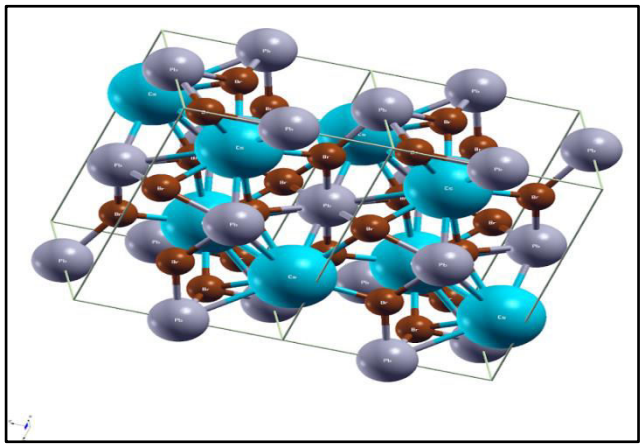

Figure-3. $CsPbBr_3$ orthorhombic crystal system obtained by computational calculations.

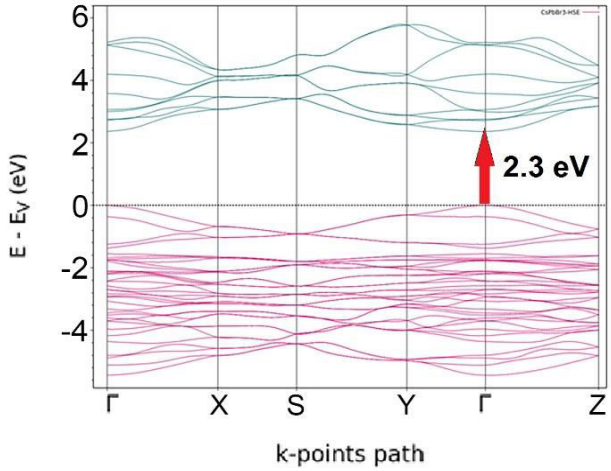

Figure-4. Band structure diagram calculated for $CsPbBr_3$.

Optical Properties

The optical properties of the material were analyzed by reflectance spectroscopy. Figure-5-a shows a reflection maximum of incident light from approximately 527 nm, which is related to the fundamental optical electronic transition between the valence band and the conduction band. This transition will be related to the optical band gap of the material. In general, at lower wavelengths from the visible region the absorption in the material is greater, the behavior in the signal found around wavelengths from 513 to 525 nm may be due to excitonic absorptions in the material. The beginning and end of absorption is related to an energy necessary to overcome the structural defects that the material can present and that represent tail states in the valence and conduction band. This necessary energy can be determined as Urbach energy. The defects result in the formation of bandgap states that are associated with a bandgap called the Urbach tail [15]. To determine the optical properties such as absorption coefficient, optical band gap and additional data such as Urbach's energy, the results obtained in Figure-4 awere used.

The material's absorption coefficient is determined using the Kubelka Munk transform, which relates the reflectance value (R) at different wavelengths with the absorption (K) and dispersion (S) coefficients. According to the following equation:

$$\frac{K}{S} = \frac{(1 - R(\lambda))^2}{2R(\lambda)}$$

the term K/S, which is also denoted as F(R), can be taken as the absorption coefficient from reflectance, the numerator is more relevant in this equation and the contribution of S is low. From the calculation of the K/S coefficient, the optical band gap of the material was determined, generating a curve equivalent to Tauc (Figure-4-b). The Tauc method is based on the assumption that the energy-dependent absorption coefficient can be expressed by the following equation:

$$(\mathrm{F(R)}.h\nu)^{1/\gamma} = B(h\nu - E_g)$$

The value of γ is 0.5, because the nature of the electronic transitions in $CsPbBr_3$ correspond to direct band transitions [16] as can be observed in the computational calculation. In Figure-5-b we observe the tauc curve for a direct band gap material, the extrapolation in the x axis of the linear behavior that corresponds to the electronic transition, it is possible to determine the optical band gap of the material which is of 2.31 eV, which is corroborated by photoluminescence measurements as shown in Figure-5-a, since the maximum intensity is at approximately in 537 nm, which corresponds to a photon energy of 2.30 eV. The behavior prior to the fundamental absorption is due to the presence of bound excitons that present a coulombian interaction between the excited electron-hole pair [17]. The magnitude of the material's absorption coefficient is $6x10^4 cm^{-1}$ for the fundamental absorption, which is adequate because values of the order of $10^5 cm^{-1}$ are expected. For wavelengths in the near UV absorption coefficients of $5x10^4 cm^{-1}$ are obtained. The expected behavior of the absorption coefficient as a function of energy is obtained, which is lower at wavelengths that are above the fundamental absorption.

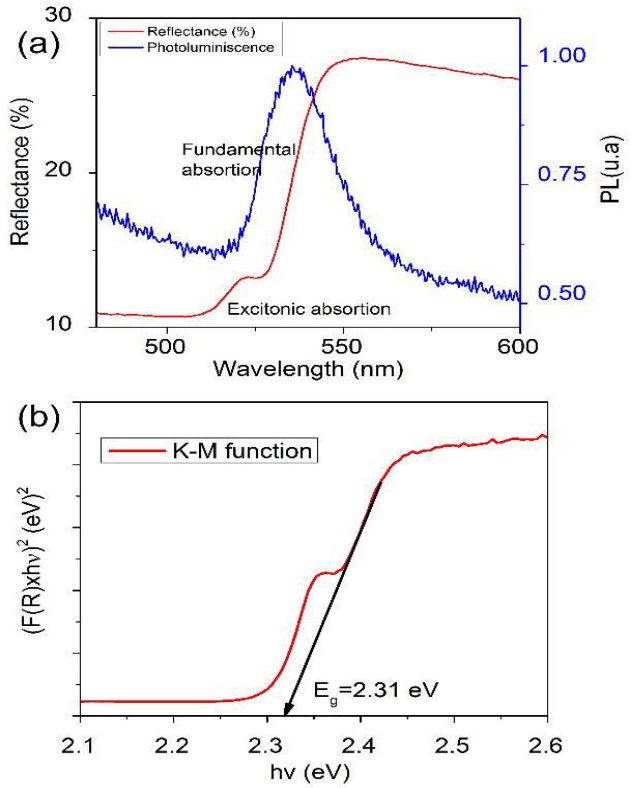

Figure-5. (a) Percentage of reflectance of $CsPbBr_3$ as a function of wavelength, (b) Tauc curve for a direct band gap material.

Finally, the Urbach energy is determined by linearizing the absorption coefficient as a function of the energy, this behavior follows an equation of the form.

$$\alpha = \alpha_g exp\left[\frac{h\nu - E_g}{E_0}\right]$$

Where E_0 corresponds to the Urbach energy which is related to the Boltzmann constant and the temperature through the KT relation [17]. As can be seen, the Urbach energy is a low value compared to the band gap calculated previously, however it is an energy value that must also be overcome to generate a fundamental electronic transition in the material. The linear correlation coefficient suggests that the data obtained follow the linear behavior of the equation used.

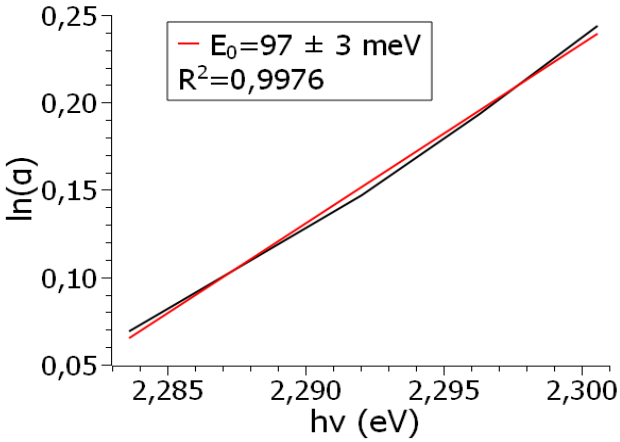

Figure-6. Determination of Urbach's energy by linear regression of the absorption coefficient as a function of energy.

CONCLUSIONS

Using a low-cost Dip Coating prototype, a thin film corresponding to an inorganic $CsPbBr_3$ perovskite was synthesized, presenting an orthorhombic crystalline system. A synthesis method was found with suitable parameters of immersion time and annealing time to obtain a material with the desired stoichiometry. The study of the film surface shows an increase in the grain size after the annealing temperature of the $PbBr_2$ film and also a change in the grain size distribution function during the synthesis process of the material of interest. This study has an influence on the electronic properties that can be studied later in the research group. The results of analysis by optical reflectance, Tauc curves, characterization by X-ray diffraction and the results of morphological analysis by SEM, allow to affirm that it is possible to synthesize a $CsPbBr_3$ film by a low-cost technique (Dip Coating) that presents parameters adequate absorption coefficients and an energy gap corresponding to a material that can be used in tandem cells. In addition, these results suggest the synthesis of materials in which the nature of the halogen can be varied in order to adjust the energy gap to lower values or try new energy gap values, which provides a material with greater potentialities.

ACKNOWLEDGMENTS

This work was partially financed by a proyect INNOVA (Hermes Code 49264) of Universidad Nacional de Colombia Sede Bogotá.

REFERENCES

[1] R. Syafinar, N. Gomesh, M. Irwanto, M. Fareq, and Y. M. Irwan. 2015. FT-IR and UV-VIS Spectroscopy Photochemical Analysis of Dragon Fruit. ARPN Journal of Engineering and Applied Sciences. 10(15): 6354-6358.

[2] J. Zhao, A. Wang, M. A. Green, and F. Ferrazza. 1998. 19.8% efficient 'honeycomb' textured multicrystalline and 24.4% monocrystalline silicon solar cells. Appl. Phys. Lett. 73(14): 1991-1993.

[3] C. R. Kalaiselvi, N. Muthukumarasamy, D. Velauthapillai, M. Kang and T. S. Senthil. 2018. Importance of halide perovskites for next generation solar cells - A review. Mater. Lett. 219: 198-200.

[4] A. Djurisic, F. Liu, H. Tam, M. Wong. 2017. Perovskite solar cells - An overview of critical issues. Progress in Quantum Electronics, Elsevier. 53: 5.

[5] G. Niu, X. Guo, L. Wang. 2015. Review of Recent Progress in Chemical Stability of Perovskite Solar Cells. Journal of Materials Chemistry. p. 2.

[6] G. Tong, L. K. Ono and Y. Qi. 2020. Recent Progress of All-Bromide Inorganic Perovskite Solar Cells. Energy Technol. 8(4): 1900961.

[7] S. M. H. Qaid, F. H. Alharbi, I. Bedja, M. K. Nazeeruddin and A. S. Aldwayyan. 2020. Reducing Amplified Spontaneous Emission Threshold in CsPbBr3 Quantum Dot Films by Controlling TiO2 Compact Layer. Nanomaterials. 10(8).

[8] J. Puetz, M.A. Aegerter. 2004. Dip Coating technique. Sol-gel technologies for glass producers and users. Springer Science Business Media New York. p. 37.

[9] F. De Matteis et al. 2019. Optical Characterization of Cesium Lead Bromide Perovskites. Crystals. 9(6).

[10] C. Tenailleau, S. Aharon, B. Cohenb, L. Etgar. 2018. Cell refinement of $CsPbBr_3$ perovskite nanoparticles and thin films. Nanoscale Advance, Royal Society of Chemistry. 1: 149.

[11] C. Lin et al. 2020. Facile synthesis of a dual-phase CsPbBr3-CsPb2Br5 single crystal and its photoelectric performance. RSC Adv. 10(35): 20745-20752.

[12] S. Zhang, Z. Yan, Y. Li, Z. Chen and H. Zeng. 2015. Atomically Thin Arsenene and Antimonene: Semimetal-Semiconductor and Indirect-Direct Band-Gap Transitions. Angew. Chemie Int. Ed. 54(10): 3112-3115.

[13] L. Atourki, E. Vega, M. Mollar, B. Marí, H. Kirou, K. Bouabid, A. Ihlal. 2017. Impact of iodide substitution on the physical properties and stability of cesium lead halide perovskite thin films $CsPbBr_{3-x}I_x$ ($0 \leq x \leq 1$). Journal of Alloys and Compounds, Elsevier. 702: 404.

[14] W. Chen, J. Zhang, G. Xu, R. Xue, Y. Li, Y. Zhou, J. Hou, Y. Li. 2018. A Semitransparent Inorganic Perovskite Film for Overcoming Ultraviolet Light Instability of Organic Solar Cells and Achieving 14.03% Efficiency. Advanced Materials, Wiley Library. 30: 2.

[15] A. Kronemeijer, V. Pecunia, D. Venkateshvaran, M. Nikolka, A. Sadhanala, J. Moriarty, M. Szumilo, H. Sirringhaus. 2014. Two-Dimensional Carrier Distribution in Top-Gate Polymer Field-Effect Transistors: Correlation between Width of Density of Localized States and Urbach Energy. Advanced Materials. 26: 730.

[16] S. M. H. Qaid, H. M. Ghaithan, B. A. Al-asbahi and A. S. Aldwayyan. 2021. Investigation of the Surface Passivation Effect on the Optical Properties of CsPbBr 3 Perovskite Quantum Dots. Surfaces and Interfaces. 23(January): 100948.

[17] S. Wasim, G. Marín, C. Rincón, G. Sánchez, A. Mora. 1998. Urbach's tails in the absorption spectra of $CuInTe_2$ single crystals with various deviations from stoichiometry. Journal of applied physics. 83: 1.